AD-A278 474

DOCUMENTATION PAGE

Form Approved OMB No. 0704-0188

2. REPORT DATE	3. REPORT TYPE AND DATES COVERED
December 1993	Final April 1990 - December 1993

4. TITLE AND SUBTITLE
Control and Management of Unsteady and Turbulent Flows

5. FUNDING NUMBERS
PE - 61102F
PR - 2307
SA - BS
G - AFOSR-90-0173

6. AUTHOR(S)
H. Nagib, M. Acharya, T. Corke, C. Wark and D. Williams

7. PERFORMING ORGANIZATION NAME(S) AND ADDRESS(ES)
Illinois Institute of Technology
Fluid Dynamics Research Center
10 W. 32nd St.
Chicago, IL 60616

8. PERFORMING ORGANIZATION REPORT NUMBER
AFOSR-TR- 94 0190

9. SPONSORING/MONITORING AGENCY NAME(S) AND ADDRESS(ES)
AFOSR/NA
Building 410
Bolling AFB, DC 20332-6448

10. SPONSORING/MONITORING AGENCY REPORT NUMBER
AFOSR-
90-0173

3004

11. SUPPLEMENTARY NOTES

12a. DISTRIBUTION/AVAILABILITY STATEMENT
Approved for public release;
distribution unlimited

12b. DISTRIBUTION CODE

13. ABSTRACT (Maximum 200 words)

Active input of tuned and detuned two-dimensional and oblique modes in a laminar boundary layer was found to lead to the growth of near-subharmonic modes as well as numerous sum and difference modes, thereby emulating "natural" transition. Acoustic receptivity of laminar boundary layers with non-localized low-amplitude periodic waviness was experimentally investigated and compared favorably to theoretical predictions. Closed loop excitation of axisymmetric and azimuthal modes in a free round jet were used to reveal the character of high Reynolds number transition (i.e., supercritical Hopf bifurcation) and to study mode selection and switching. Suction and blowing were shown to be capable of controlling the asymmetric flow about the forebodies of aircraft and missiles and the experiments indicate that the suction bleed coefficient must increase like the 3.9 power of the velocity to balance the effects of geometric instability at the tip. The effects of yaw on such asymmetries were also documented. A strategy to suppress the dynamic-stall vortex over a range of operating parameters, using controlled leading-edge suction to prevent accumulation of reverse-flowing fluid, was successfully developed from a study of the mechanisms responsible for the evolution of the vortex. The National Diagnostic Facility was completed and several collaborative experiments are scheduled during 1994.

14. SUBJECT TERMS
Turbulence, Separated Flows, Unsteady Flows, Transition
Forebody Flows, Pitching Airfoils, Jet Flows, Control

15. NUMBER OF PAGES
30

16. PRICE CODE

17. SECURITY CLASSIFICATION OF REPORT	18. SECURITY CLASSIFICATION OF THIS PAGE	19. SECURITY CLASSIFICATION OF ABSTRACT	20. LIMITATION OF ABSTRACT
Unclassified	Unclassified	Unclassified	UL

NSN 7540-01-280-5500

Standard Form 298 (Rev. 2-89) Prescribed by ANSI Std. Z39-18 298-102

Table of Contents

Page

Abstract

Active input of tuned and detuned two-dimensional and oblique modes in a laminar boundary layer was found to lead to the growth of near-subharmonic modes as well as numerous sum and difference modes, thereby emulating "natural" transition. Acoustic receptivity of laminar boundary layers with non-localized low-amplitude periodic waviness was experimentally investigated and compared favorably to theoretical predictions. Closed loop excitation of axisymmetric and azimuthal modes in a free round jet were used to reveal the character of high Reynolds number transition (i.e., supercritical Hopf bifurcation) and to study mode selection and switching. Suction and blowing were shown to be capable of controlling the asymmetric flow about the forebodies of aircraft and missiles and the experiments indicate that the suction bleed coefficient must increase like the 3.9 power of the velocity to balance the effects of geometric instability at the tip. The effects of yaw on such asymmetries were also documented. A strategy to suppress the dynamic-stall vortex over a range of operating parameters, using controlled leading-edge suction to prevent accumulation of reverse-flowing fluid, was successfully developed from a study of the mechanisms responsible for the evolution of the vortex. The National Diagnostic Facility was completed and several collaborative experiments are scheduled during 1994.

Introduction

Unlike most other research environments working in fluid dynamics, the members of the FDRC at IIT work in a cohesive group atmosphere. By this approach we make use of a centralization of facilities, equipment and computer capabilities in a manner which has the greatest impact on productivity in the widest possible breadth of problems and flowfields. The group is made up of six faculty members, post-doctoral research associates, support staff and research assistants. The five Principal Investigators of this program were joined by Professor Richard Wlezien, who is currently with NASA-Langley Research Center, during most of the three year period. Dr. Patrick Reisenthel was instrumental in guiding some of the early student work in the free-jet facility before joining NEAR Inc. The support staff at FDRC includes Marion Denne, the center secretary, Edward Nieman, the center facilities coordinator, and Dominic DeLuca, the center electronics technician. As Facilities Coordinator, Ed Nieman has the responsibility for maintaining all of the research facilities, as well as aiding in the design and manufacturing of models, probes and other additions or modifications required for our experiments. For example, he has played an integral role in the implementation of the design and construction of the National Diagnostic Facility. He is assisted in his functions by Craig Johnson. Both of them deserve a great deal of credit in the completion of the National Diagnostic Facility wind tunnel during this grant period. As electronics technician, Dominic Deluca's responsibilities include maintaining electronic equipment and computer systems, as well as aiding in the design of specialized instrumentation, building of prototypes and mass production of multiple components.

The research activities are summarized in the following section under six topics. These topics and the investigators responsible for them are:

A. Broadband 3-D Mode Development in a Blasius Boundary Layer by Resonant Mode Detuning	T. Corke
B. Acoustic Receptivity of Laminar Boundary Layers Over Wavy Walls	R. Wlezien & H. Nagib
C. Dynamics of Free Jets in Presence of Enhanced Feedback with Multiple Azimuthal Modes	T. Corke, P. Reisenthel & H. Nagib
D. The Effect of Yaw and the Control of Forebody Vortex Asymmetry	D. Williams & C. Wark
E. Flow Control About Pitching Airfoils at High Angles of Attack	M. Acharya
F. The National Diagnostic Facility	H. Nagib, T. Corke, R. Wlezien M. Acharya, D. Williams & C. Wark

Summary of Results

A. Broadband 3-D Mode Development in a Blasius Boundary Layer by Resonant Mode Detuning

This work involves the simultaneous input of a plane TS wave with wave numbers along with pairs of oblique waves with equal but opposite spanwise wave numbers in order to study the secondary growth of three dimensional modes in a Blasius boundary layer. In our earlier work (Corke and Mangano, 1989 and Corke, 1990), the frequency of the oblique modes was exactly the subharmonic of the plane TS mode. These modes were also phase locked. This so-called subharmonic mode transition lead to a resonant growth of the otherwise linearly damped oblique waves as well as the growth of higher harmonic 3-D modes. In the present work we start with initial modes which are not harmonically related in frequency. Such "detuned" conditions also lead to the secondary growth of the initial 3-D mode. In addition it promotes the growth of numerous discrete modes produced by sum and difference interactions. These interacted modes are also three dimensional. Because each generation of interacted modes has a higher amplification rate than the previous, the spectrum rapidly fills towards a broad-band character. The process of growth of these modes also lowers the maximum amplitude reached by the primary 3-D mode compared to a "tuned" interaction. This scenario is of interest because it provides a mechanism for the generation of a broad spectrum at the later stages of subharmonic mode transition, and is possibly more relevant to conditions of "natural" transition where low amplitude broad-band disturbances seed the initial modes and an exact fundamental-subharmonic interaction is unlikely.

Background. It is now well established that the principle route to transition in a 2-D boundary layer, having a linear growth regime, and in the absence of a strong adverse pressure gradient, is by a resonant interaction between a triad of modes made up of a plane TS wave and pairs of oblique waves with equal-opposite wave angles. If all the modes are eigensolutions of the Orr-Sommerfeld equation, then the three wave resonance is of a specific type first postulated by Craik (1971). Because this usually involves oblique modes at the subharmonic frequency of the plane mode, it is often referred to as subharmonic transition. Because it involves initially linear modes, it can occur at very low initial amplitudes. With slightly higher initial amplitudes, a different and more general mechanism for the first growth of three dimensionality comes into play. This was first presented by Herbert (1983). It involves the secondary instability of a basic flow made up of the mean flow and plane TS wave subject to spanwise periodic vorticity perturbations corresponding to Squire modes. This mechanism allows a spanwise wave number selectivity that is not present in Craik's approach. The results of our early investigations (Corke and Mangano (1989) and Corke (1990) have verified this wave number selectivity as well as the eigenfunction structure of the principle and interacted modes up to and past the point of energy saturation. We had also shown that the process of transition in these cases was fundamentally different from that associated with the earlier experiments such as by Klebanoff et al. (1962) which introduced a high (approximately 1% u'/Uo) initial amplitude plane TS wave. In those early experiments, the large TS forcing resulted in the development of an inflexional mean velocity profile in a thin shear layer away from the wall, in the outer part of the boundary layer. As a result of an inviscid instability, higher frequencies were produced which lead to a rather fast and violent "breakdown" to turbulence. In our cases, starting with low initial amplitudes (approximately 0.07% u'/Uo) so that the initial modes pass through a linear growth stage, we do not observe inflexions in the

mean velocity profile or high frequency "spike stages" associated with an inviscid instability. Rather, we observe a gradual spectral broadening at low, intermediate and higher frequencies. We have attributed this to a process of "mode detuning" whereby the initially exact fundamental-subharmonic interaction becomes gradually detuned leading to the generation of frequency side bands. These side band modes derive energy from the primary modes, and through sum and difference interactions produce new modes. Each successive generation of modes interacts with the others until the spectrum becomes relatively broad-band. A bellwether of this process is the appearance of a low frequency component corresponding to the lowest difference mode. Such an increase in the energy in velocity fluctuations at low frequencies had been observed in the experiments of Kachanov and Levchenko (1984). This was seen as a low frequency amplitude modulation of the subharmonic mode. In their case they had only input a plane TS wave. The subharmonic mode that developed had grown out of the background disturbances. They believed that the growth of the broad band of lower frequencies was due to stochastic modulation of the phase and amplitude of the subharmonic mode. In an effort to explain these observations, Santos and Herbert (1986) and Santos (1987) examined the secondary instability of the mean flow and fundamental TS wave to a "detuned" subharmonic 3-D perturbation. For this they found a broad peak of amplification which they felt could produce a similar type of low frequency beating observed by Kachanov and Levchenko. As with our earlier experiments, we introduced both 2-D and 3-D disturbances into the boundary layer in order to seed simultaneously a plane TS wave and oblique wave pairs. For studying detuned interactions we have used 3-D modes with a spanwise wave number which matches that of the most amplified case of Corke and Mangano (1989). In that work, the tuned fundamental/subharmonic dimensionless frequencies were F=79/39.5. For the detailed experiments with mode detuning, the frequency of the 3-D mode was maintained at F=39.5. The frequency of the 2-D mode was increased to F=88.9. For these conditions, a parametric study was done to investigate the effect of initial amplitudes of both the primary 2-D and 3-D modes. Also the effect of the amount of frequency detuning was investigated in a separate series of experiments (Koratagere, 1991). These studies helped to explain some of the fundamental aspects of detuned subharmonic resonance, as well as provide such initial conditions as the initial amplitudes to be used during the detailed velocity surveys. These measurements provided quantitative information regarding streamwise wavenumbers, wave velocities and spatial amplification rates of the primary and interacted modes. Velocity surveys in three space directions were also done in order to reconstruct the flow field in a phase averaged sense. These were then compared to similar measurements with an initially tuned fundamental/subharmonic interaction.

Sample results. A sample of some of the results is presented in Figures 1 to 4. Figure 1 contrasts spectra of streamwise velocity fluctuations for exact (top) and detuned (bottom) fundamental/subharmonic interactions. For these, the primary 3-D mode had a physical frequency of 16Hz. For the detuned condition, the physical frequency of the 2-D mode was 36Hz. In both cases the primary 3-D mode grew through a resonant energy exchange with the primary 2-D mode. However in the detuned case, this process also lead to the growth of numerous sum and difference modes. The first of these modes to be produced was the harmonic of the 3-D mode at 32Hz and the difference mode at 20Hz (36-16). Following these, the lowest difference frequency at 4Hz (36 -32) appeared. The other modes develop from these through other sum and difference interactions with the primary 3-D mode and its harmonics. Cross-spectral measurements of velocity fluctuations at locations spaced in the flow direction showed that except for the initial 3-D mode and its harmonics, the interacted modes were traveling at

different phase speeds. This is illustrated by the linear coherence function shown as the dotted curve at the top of Figure 2. The dashed and solid curves in the figure correspond to auto-spectra for respective u-velocity time series at the upstream and downstream locations used for the cross statistic. These were at the spanwise and wall normal positions where the u-fluctuation amplitudes were a maximum. For all the modes seen in the spectrum, only the primary 3-D mode at 16Hz, and it harmonics (32Hz in the range of frequencies shown) were linearly phase locked (having a coherence value of 1). In our experiments, where the same phase clock that introduces the initial modes was used to acquire the time series, a high linear coherence between modes sampled at two x-locations signifies a matching in phase speeds. In order to see how the other modes in the spectrum are related to the linearly phase locked modes, we look at the normalized third order cross-spectrum or cross-bicoherence (CBC). The cross-bicoherence is a measure of triple phase locking, $\theta(f_1)+\theta(f_2)-\theta(f_3)$=constant, that exists from realization to realization. $\theta(f1)$ is the instantaneous phase angle of the Fourier transformed time series, $u_i(f)$ The CBC for the same time series used in the auto-spectra is shown in the bottom part of Figure 2. To satisfy the Nyquist criteria, the region of validity of the CBC takes the form of the bold outlined triangles. By our convention, the frequencies at the upstream position are read from the abscissa. Those at the downstream position are read on the ordinate. The third frequency also corresponds to the downstream position, and it is read as the intercept of a -45° line to the abscissa. The magnitude of the CBC is drawn as constant level contours with values of 0.35, 0.65 and 0.85. The CBC in Figure 2 indicate a nearly perfect quadratic phase locking between the discreet modes at the upstream and downstream positions. An important observation is that the peaks in the CBC for the different modes are all aligned under the linear phase locked modes (16 and 32Hz). This indicates that the other modes are phase locked only through an interaction with one or both of these two modes. An example of how this process occurs is highlighted by the arrows in the figure. Through a difference interaction, the lowest difference mode at 4Hz interacts with the primary 3-D mode at 16Hz and the interacted mode at 12Hz, as well as with the mode at 32Hz and 28Hz. Through a summing interaction, the 4Hz mode also interacts with the 16 and 32Hz modes to produce modes at 20 and 36Hz, respectively. For those modes that have a statistically significant CBC, we can determine the cross-biphase. Figure 3 shows (bottom) the streamwise development of the cross-biphase for the 4Hz mode. Shown at the top of the figure are the CBC values. Because the 4Hz mode can be derived by two interactions (16-12 and 32-28) we have two sets of data points. For each set, the streamwise development falls on a straight line. The slope of the lines corresponds to the streamwise wave number for the mode. Since in both sets the frequency is the same, this indicates that there are two modes with different streamwise wave numbers (streamwise wave lengths) which produce a frequency of 4Hz. In fact this is the case for all of the interacted modes. Figure 4 gives a table of some of the dominant modes along with their streamwise wave numbers, phase speeds and streamwise wave lengths. This shows that the linear phase locked modes have the same phase speeds. The phase speed of the primary 2-D mode is close these thus satisfying the condition for combination resonance. The other modes have phase speeds significantly faster and slower than these modes. However, the wave lengths of these modes are all comparable to that of the initial 2-D or 3-D modes. Thus we observe a scenario which is the opposite of a wave packet, namely, rather than waves of different wave lengths traveling at comparable speeds, we have waves of comparable wave lengths traveling at different speeds. We generally find that the mechanism of detuning of secondary 3-D modes in a boundary layer provides all the necessary conditions for rapid broad-band 3-D mode growth. Importantly, it can start from low initial amplitudes which are relevant to natural (stochastically forced) boundary layers.

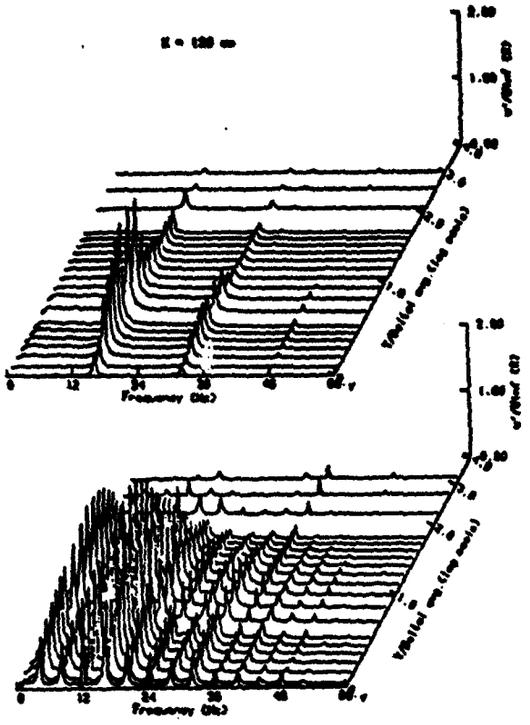

Figure 1. Comparison of u-component spectra for "tuned" (top) and "detuned" (bottom) subharmonic 3-D mode resonance.

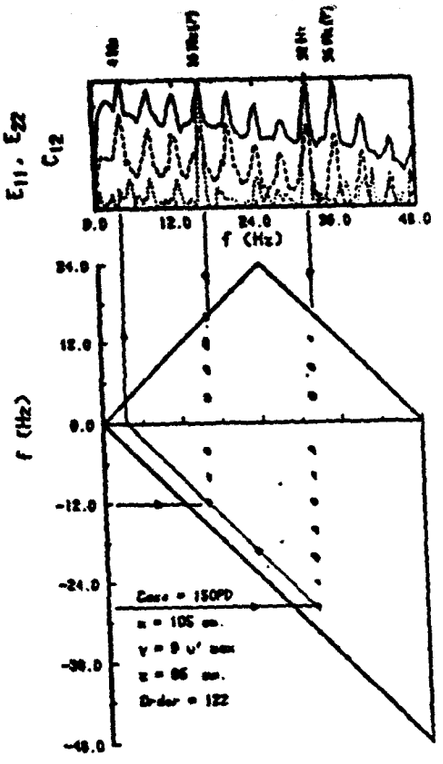

Figure 2. Auto-spectra and linear coherence (top) and cross-bicoherence (bottom) for a u-time series with respect to an upstream reference for "detuned" conditions.

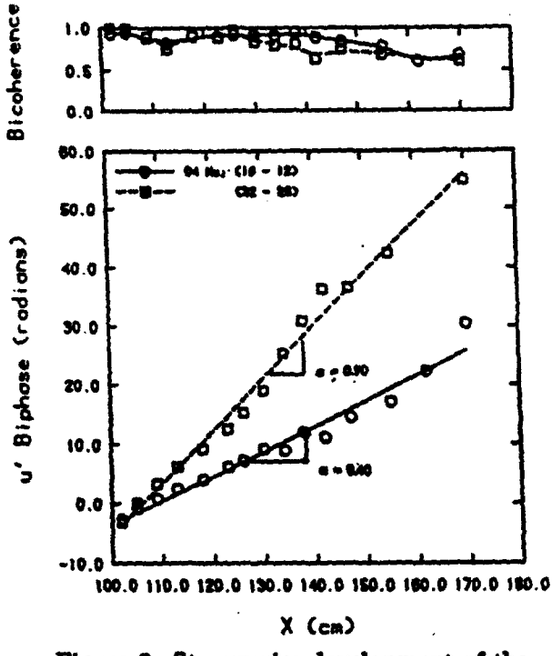

Figure 3. Streamwise development of the cross-biphase for the lowest difference frequency (4Hz.) for "detuned" conditions.

Frequency (Hz)	Streamwise Wave No. $\alpha(cm^{-1})$	C_r/U_∞	Streamwise Wavelength $\lambda_x=2\pi/\alpha$ (cm)	Interaction
16	0.45	0.37	13.96	———
32	0.87	0.37	07.22	16 + 16
48	1.32	0.37	04.76	32 + 16
36	0.93	0.39	06.76	32 + 04
04 (a)	0.42	0.10	14.95	16 - 12
04 (b)	0.88	0.05	07.13	32 - 28
08 (a)	0.92	0.09	06.83	32 - 24
08 (b)	0.62	0.13	10.13	16 - 08
12 (a)	0.41	0.30	15.32	16 - 04
12 (b)	0.99	0.12	06.35	32 - 20
20 (a)	0.82	0.25	07.66	16 + 04
20 (b)	0.97	0.20	06.47	32 - 12
24 (a)	0.67	0.36	09.38	16 + 08
24 (b)	1.00	0.24	06.28	32 - 08
28 (a)	0.79	0.36	07.95	16 + 12
28 (b)	0.93	0.30	06.76	32 - 04
40	0.95	0.42	06.61	16 + 24
44	1.00	0.44	06.28	32 + 12

Figure 4. Table of wave lengths and phase speeds for primary and interacted modes for "detuned" conditions.

B. Acoustic Receptivity of Laminar Boundary Layers Over Wavy Walls

The process of transition in boundary layers can roughly be divided into three stages: receptivity to external disturbances followed by exponential growth (typically predicted by linear theory) and finally (if sufficient amplitude is achieved) nonlinear breakdown through secondary instabilities. A conventional approach to predicting boundary-layer transition is the determination of the location at which the boundary layer becomes linearly unstable to spatially and/or temporally growing instabilities. When the total amplification of a range of disturbance frequencies exceeds a threshold level (typically e^N) transition is said to occur. Inaccuracies in these methods can be attributed to the inability to predict initial disturbance amplitudes, secondary instabilities, three dimensional modes, and interaction among modes. More recent numerical approaches (such as the parabolized stability equations, PSE) can account for the linear and nonlinear growth of disturbances in boundary layers, but the initial disturbance levels must still be known. Receptivity thus plays a crucial role in the refinement of transition prediction techniques.

In general, the receptivity mechanism at distributed inhomogeneities is similar to that for localized roughness if one considers the total receptivity to be the sum of contributions from a series of infinitesimal subdomains. Choudhari (1993) discusses analytical work on distributed receptivity, beginning with the work of Zavol'skii et al (1983). Distributed roughness can be classified as either periodic, involving only a limited number of discrete Fourier modes, or nonperiodic, where the roughness distribution is arbitrary. The general approach to an arbitrary nonlocalized roughness distribution is provided by Choudhari (1992). Receptivity over periodic two-dimensional wall roughness is addressed by Choudhari (1993) and Crouch (1990). Crouch and Bertolotti (1992) extend these results using parabolized stability equations that include the effects of boundary-layer non-parallelism and show that the non-parallel effects are only significant for three-dimensional disturbances.

Theory shows that receptivity at a periodic distributed waviness has the distinguishing characteristic of tuned response. When the T-S wavelength is nearly that of the wall waviness, there is maximum energy transfer from the acoustic field to the T-S mode. Crouch (1990) shows that this response is O(10) times as great as that for localized mechanisms. However, the response rapidly becomes negligible as the T-S wavelength is detuned from that of the wall waviness. Choudhari(1993) shows that the tuned response is greater than either localized or randomly distributed roughness, with random distributions producing receptivity intermediate between localized and purely periodic roughness.

The purpose of this investigation was to directly validate the theory of acoustic boundary-layer receptivity at periodic distributed waviness. Continuous waviness was simulated by discrete tape strips arranged in a periodic array. Plane-wave acoustic forcing was used to excite a T-S response in the boundary layer, and the resulting mode shapes were measured and analyzed. It was established that a plane traveling wave is the requisite forcing field for distributed receptivity experiments, but it does not occur naturally in a closed-return wind tunnel. When the acoustic frequency was below transverse-mode cut off, a purely traveling plane wave could be established using the appropriate source configuration. A primary source was located upstream of the test section, and a secondary source downstream of the test section was used to actively cancel upstream-traveling acoustic components. It was possible to generate a forcing field that nearly approximates waves traveling downstream at zero incidence to the test plate.

After proper decomposition of the excited T-S mode from the total fluctuating velocity, a good match between the measured T-S mode shape and the theoretical T-S mode shape was observed. Other receptivity mechanisms were shown to be small compared to that due to wavy-wall receptivity, and contributions from these extraneous components were removed from the net

response. By increasing the number of wavelengths comprising the receptivity site it was shown that only a small symmetric region in the vicinity of lower branch can produce the same receptivity as an infinite wavy surface. It was also shown that the ratio between wavy-wall receptivity and the receptivity due to one strip (equivalent to the ratio between distributed and localized receptivity) is of O(10), as predicted by theory.

Strong detuning was verified by measuring the effect of mismatching the excited T-S wavelength with the wall wavelength. A mismatch of $\pm$ 10% produces negligible T-S response in the boundary layer, which is in agreement with theoretical predictions by Choudhari (1993) and Crouch (1990). Numerical calculations by Choudhari that directly simulate the freestream velocity detuning used in the present experiment show good agreement in the shapes of the curves as well as in absolute amplitude; see Figures 5, 6 and 7. It is thus possible to conclude that the theory captures the physics of the acoustic receptivity mechanism.

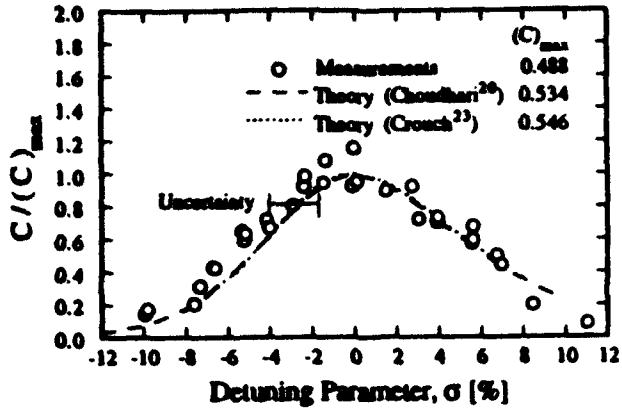

Fig. 5 Receptivity coefficient versus detuning parameter; f = 80 Hz, θ'_{ac} = 0.0014 m/s

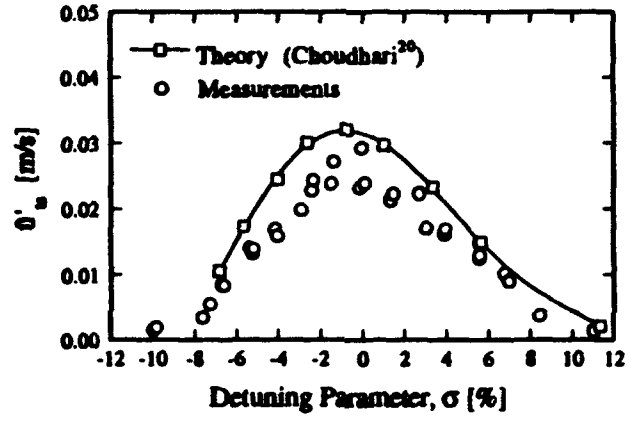

Fig. 6 Magnitude of T-S response to wavy-wall receptivity versus detuning parameter; f = 80 Hz, θ'_{ac} = 0.0014 m/s

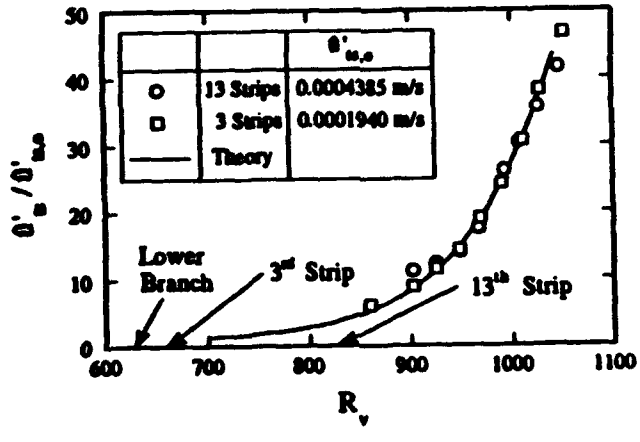

Fig. 7 Normalized T-S amplitude versus boundary-layer Reynolds number; comparison of stability theory and experiment

C. Dynamics of Free Jets in Presence of Enhanced Feedback with Multiple Azimuthal Modes

Resonance with Helical Mode Input. This work involves the active input of fundamental two and three dimensional amplified modes in an axisymmetric jet. This was done by introducing localized acoustic disturbances that are produced by an azimuthal array of miniature speakers placed close to the jet lip on the exit face. The independent control of the each speaker allows different azimuthal amplitude and phase distributions of periodic inputs The types of inputs in this study consisted of conditions to force helical mode pairs with the same frequency and equal but opposite azimuthal wave numbers, $m=\pm1$, separately, or with axisymmetric ($m=0$) modes. Three forcing conditions were studies in detail. The first consisted of a weakly amplified helical mode pair which was essentially "superposed" with the natural jet instability modes. This provided a reference to the second case which consisted of the same helical mode pairs along with an axisymmetric mode at the harmonic streamwise wave number. This was designed to lead to the resonant growth of the otherwise weakly amplified subharmonic helical mode. The third case consisted of forcing $m=\pm1$ helical mode pairs at a frequency that was close to the most amplified. This was compared to the results of Corke et al. (1991) who forced an axisymmetric mode at the same frequency and found it to lead to the growth of near-subharmonic modes, as well as numerous sum and difference modes. The use of a different mode type in the present work was intended to lead to possible mechanisms for this behavior.

This work is motivated by the fact that for an axisymmetric jet, with a thin exit shear layer compared to the radius ($r_{1/2}/\theta_i<100$), by linear theory the initial shear layer is equally unstable to both axisymmetric ($m=0$) and the first helical mode ($m= +$ or -1). Although the linear characteristics are similar, Mankbadi and Liu (1981) have shown that their nonlinear development is quite different. As a result of nonlinear effects, the streamwise life span of the first helical mode is less than that of the axisymmetric mode. However, the mechanism which limits the streamwise extent of this mode also makes it more efficient in pumping energy into fine scale turbulence. The net result is that helical modes are still more effective in enhancing turbulence than their axisymmetric counterparts.

Since the streamwise extent of growth of a mode is proportional to its wavelength (with low initial amplitudes, energy saturation occurs after approximately four wavelengths downstream), longer wavelength helical modes have a greater potential for a significant and sustaining influence on turbulent production in jets. From linear theory, such lower frequency modes are considered less important due to their lower amplification rates. However in the presence of a properly selected more amplified mode, intermodal energy transfer can lead to enhanced growth.

A sample of the results are presented in Figures 8 and 9. These correspond to input modes which consisted of $m=\pm1$ helical mode pairs at frequency f_{fh}, and an axisymmetric ($m=0$) mode at twice their frequency. The streamwise growth in amplitude of the input helical modes at different azimuthal positions is shown in Figure 8. For this data we have applied an amplitude evolution model based on a weakly nonlinear three wave resonance. The three waves are the fundamental axisymmetric mode and subharmonic helical mode pairs. The result of the analysis gives an expression for the amplitude of the helical mode A_2 as

$$A_2=A_{20}\exp\{-\alpha_{i2}x + b'\exp(-\alpha_{i3}x)\}$$

where $b'=bA_{30}/C_r\alpha_{i3}$ and A_{20} and A_{30} are reference initial amplitudes for the helical and axisymmetric modes, respectively. Physically, $b/C_r\alpha_{i3}$ represents a dimensionless coupling coefficient between the axisymmetric and helical modes. As seen in Figure 8, this evolution

equation is observed to represent well the growth of the helical mode in this case, irrespective of the azimuthal position.

The effect of the resonant growth of the helical mode on the spreading of the shear layer in this case is presented in Figure 9. This is shown from a viewpoint which illustrates the azimuthal variation of the momentum thickness at different streamwise positions (shown as different line types). When the helical mode grows to large amplitude, we expect a nonlinear interaction to result in the modification of the mean flow. For helical mode pairs with azimuthal wave numbers $\pm m$, this will produce an azimuthal variation of the mean flow with an azimuthal wave number of $\pm 2m$. Physically, for $m=\pm 1$ this will appear as a $\cos(2\gamma)$ variation of the shear layer thickness. From the viewpoint of Figure 9, this will appear as an ellipse-shaped distribution of the momentum thickness. The degree of eccentricity above 1 is a measure of the amount of mean flow distortion resulting from the growth of the helical modes.

The momentum thickness distribution for the base flow case, corresponding to the weakly amplified helical mode pairs by themselves, is shown at the top of Figure 9. Within the linear growth region (up to $x/D=0.25$) the azimuthal distribution is circular, indicating that the weakly amplified helical mode pairs input in this case were not of sufficient amplitude to distort the mean flow. Further downstream of this point, the amplitude reached by this mode does result in some degree of eccentricity, with a maximum value of 1.15 by the last x/D position.

The momentum thickness distribution for conditions to promote the resonant growth of the helical mode are shown at the bottom of Figure 9. In this case, the rapid growth in amplitude of the helical mode produces a noticable azimuthal mean flow distortion by the first measurement station. By the last x-location, the value of the eccentricity in the mean flow is 1.5. When the azimuthally summed momentum thicknesses were compared for the two cases, we measured a 300% larger value for the case of subharmonic helical mode resonance over that of the weakly amplified helical modes, or natural (unforced) shear layer.

Closed Loop Excitation. When excited under enhanced feedback conditions, the initial shear layer of a transitional subsonic free jet can be destabilized into limit cycle behavior for air speeds exceeding a critical Reynolds number. The critical Reynolds number, Re_c is dependent upon the gain of the feedback loop and the position of the feedback probe in the flowfield. In the present experiment, the latter were keep fixed, with a configuration chosen so as to minimize the possibility of frequency jumps between eigenmodes of the feedback loop.

he system was shown to undergo a supercritical Hopf bifurcation around Re_c; see Figure 10. This was demonstrated from two sets of experimental observations. First, the steady-state oscillation amplitude was found to obey the square root law from the critical point. Second, a detailed examination of the eigenvalue locus of the linearized system. parameterized by Reynolds number, revealed the proper scaling for a bifurcation of the Hopf type. These observations were made possible by a unique feature of the experimental setup; i.e., the ability to perform synchronized temporal growth experiments by electronically opening and closing the feedback loop.

Parameter identification techniques were used to test the applicability of a simple evolution equation model (the temporal Landau equation) to the global dynamics of the acoustic feedback system. The usefulness of this simplified dynamical system representation (e.g., for control purposes) relies in part on its ability to accurately characterize the state of flowfield over some region of space, rather than at a single point; see Figure 11. For the investigated range (up to 4λ), it was found that both real and imaginary parts of the linear coefficients of Landau's equation are functions of the Reynolds number only. The nonlinear Landau coefficient is

essentially real. It, however, depends strongly upon the downstream distance from the jet lip, and reflects the spatial variations of the saturation amplitude in the initial shear layer. The Landau equation for the fundamentals eigenmode is found to adequately describe the dynamics of enhanced feedback for $\chi/\lambda \leq 2$. Beyond this location in the shear layer, it is necessary to incorporate a model of the interaction between the eigenmode and its subharmonic.

From a flow control perspective, the validation of simplified model evolution equations is a potentially powerful tool. Examples of flows where this research may find applications include: impinging jets, flow over cavities, and possibly, jet screech.

Azimuthal mode selection with enhanced feedback. Here we have investigated the role of nonlinear effects and pressure feedback on the selection of fundamental axisymmetric and helical modes in the initial shear layer of an axisymmetric jet. For this we used the technique of enhanced feedback whereby vortical fluctuations occurring in the shear layer downstream are electronically fed back and converted into pressure fluctuations at the jet lip. In our approach the fed back signal is made up of different combinations of azimuthal mode types. The selection of one mode over another is determined in part by the feedback gain consisting of the linear stability spatial amplification rate and electronic gain. With large enough feedback gain, one mode can be set to dominate over others. The more interesting condition corresponds to an intermediate setting for which mode switching, similar to what we have observed in natural jets, is found to occur. The documentation of these different regimes, and the modelling of the interactions between higher azimuthal number modes ($m=\pm 5$ & 6) is a primary focus of this work.

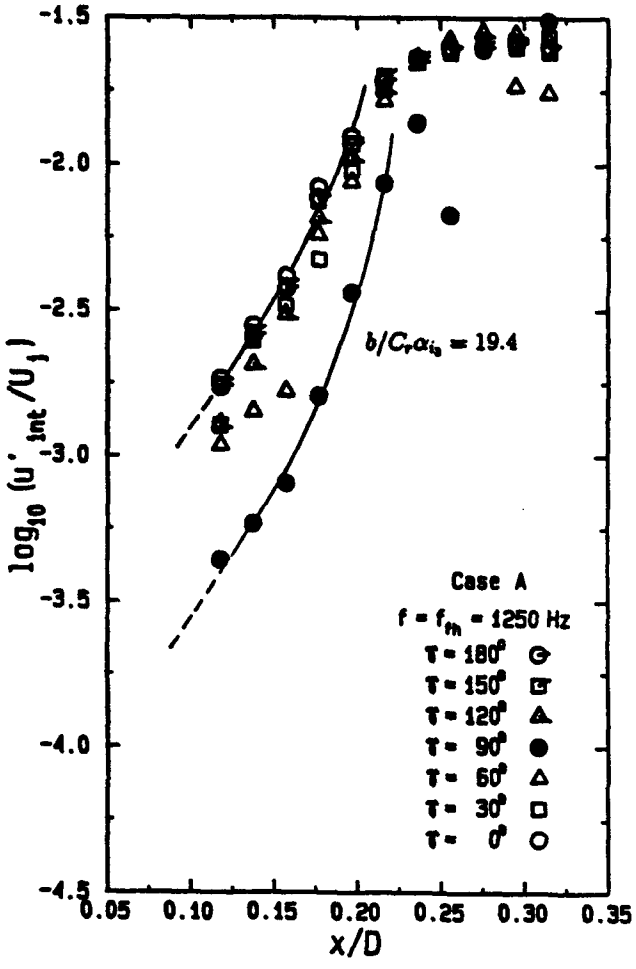

Figure 8 Streamwise growth in amplitude of helical mode at different azimuthal positions (points) and comparison to three-wave resonance amplitude model (curve).

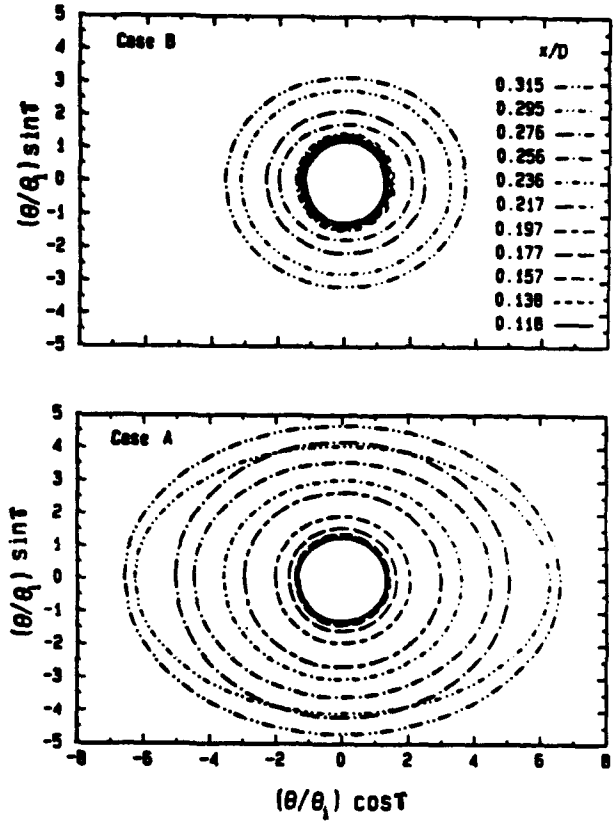

Figure 9 Streamwise development of azimuthal variation in momentum thickness for weakly amplified helical mode alone (top) and combined with an axisymmetric mode at the harmonic frequency (bottom).

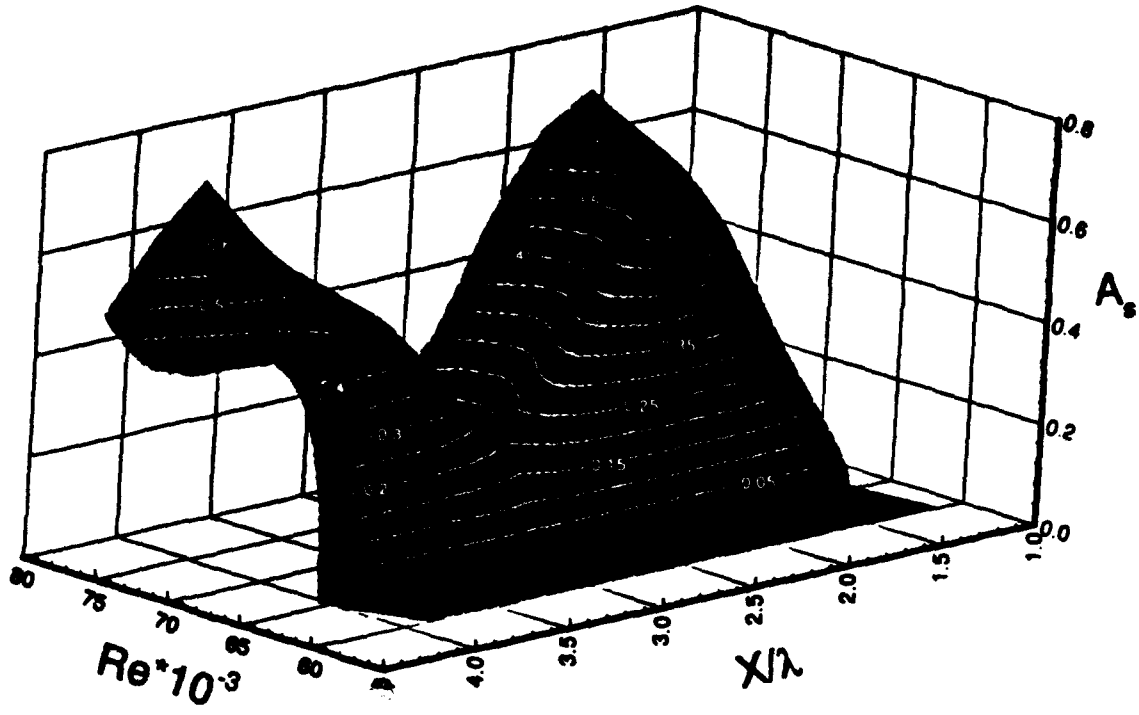

Fig. 10 Curve Fit Representation of the Global Hopf Bifurcation in Space, Around $Re_c = 65{,}500$.

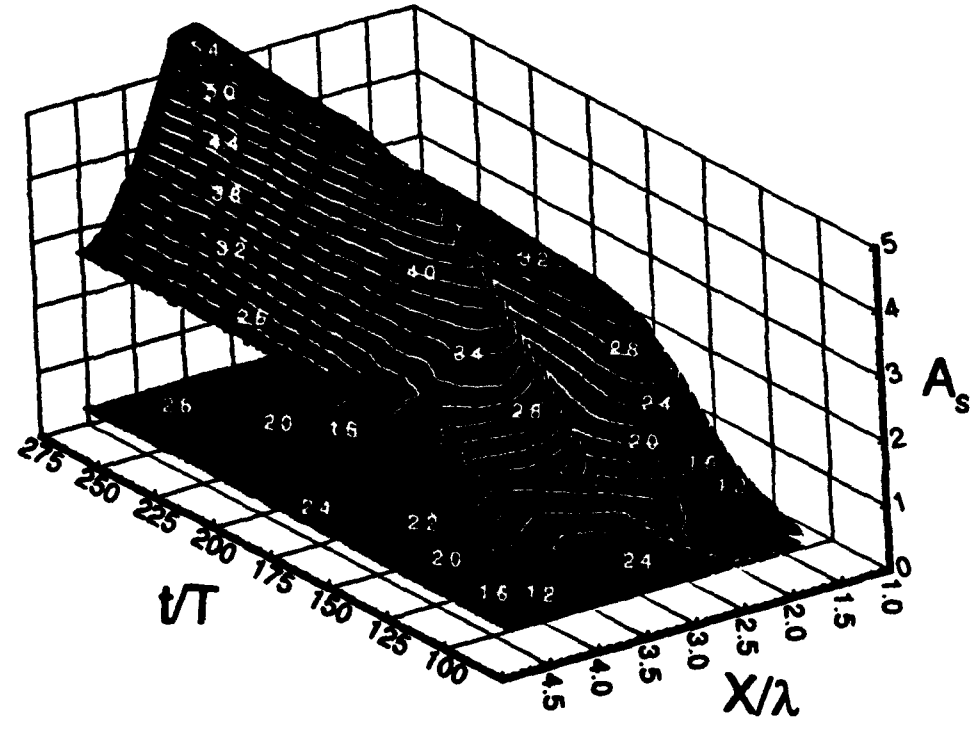

Fig. 11 Three-Dimensional Diagram Representing the Spatio-Temporal Evolution of Both Fundamental and Subharmonic Frequencies at $Re = 76{,}000$. (Projected Contours in the Plane $A_s = 0$ Correspond to the Fundamental).

D. The Effect of Yaw and the Control of Forebody Vortex Asymmetry

Yaw Effects. Aircraft and missiles encounter very strong side forces, during maneuvers at high angles of attack. This side force is very difficult to control and many investigations have recognized this force as a result of the asymmetric vortex separation occurring on the lee side of a slender body of revolution. A large number of parameters influencing this phenomenon have been studied, but many problems persist and this investigation focuses on the effect of yaw on the vortex separation.

There is a general consensus about the description of the flowfield on the lee side of a stationary pitched slender body of revolution. Although model geometry has a dramatic influence on the wake, common gross characteristics can still be extracted by comparing the flow behind different model configurations. An investigation by Montividas (1988) provides visualization of the different flow regimes encountered by a slender body of revolution. When a stationary cone-cylinder model is placed at angles of attack ranging from 0° to 90°, three succe regimes were identified and documented. The first regime occurs when the cylinder is pitch he range $0° < \alpha < \alpha_a$ (where α is the pitch angle and α_a is the angle of the onset of asymmetric vortex separation). Model geometry dependent, α_a ranges between 30° and 50°. At very low angles of attack, there is no separation of the boundary layer on the lee side. At higher angles of attack up to $\alpha = \alpha_a$, the component of the freestream velocity perpendicular to the cylinder (crossflow) increases thereby causing the boundary layer to separate, rolling up into two symmetric counter-rotating vortices. For this regime there is no net side force.

The second regime is observed in the range $\alpha_a < \alpha < \alpha_u$ where α_u will be discussed below. The crossflow dominates and it is believed that a small instability triggered near the tip of the cylinder causes the vortices to separate asymmetrically. This resulting pressure difference between the two sides of the cylinder caused by the asymmetric vortex separation, induces a side force. The vortices present in this regime are steady and alternately separate from either side along the model. The number of vortices depends on the angle of attack and on the aspect ratio (L/D). The first separating vortex will be referred to as the primary vortex and the second separating vortex will be called secondary. When α is larger then α_u (angle of onset of the unsteady regime) unsteady separation of vortices occurs on the lee side of the model. Unsteady shedding results in an unsteady side force, with the time average side force being approximately equal to zero.

One must keep in mind, that the transition between the regimes is continuous. In fact, for large aspect ratios all three regimes can be present along the length of the cylinder. Secondly, two models, the same in appearance will not have the same α_a and α_u. Keener and Chapman (1974) showed that for the same tip, the larger the aspect ratio the smaller the angle of onset of asymmetry. Also the aspect ratio will determine the number of vortices that will separate from the cylinder.

Of more importance to the present investigation is the effect of the pitching motion. A very intensive study by Montividas (1988) maps the onset angles of the different flow regimes over nondimensionalized constant sweep rates ω' ($-0.375 < \omega' < 0.375$). The major conclusions found from this study were that the three regimes are still present over the whole range of sweep rates investigated and it was also found that positive sweep delays the angle of onset of asymmetry, whereas the opposite is true for negative sweeps.

Using a copy of Montividas' blunt cone-cylinder model and flow visualization technique, the effect of both positive and negative yaw on the flow field behind the model is studied both in the steady case and pitching case. Isolating the effects of this parameter can lead to a better overall understanding of the asymmetric vortex separation process. The emphasis was put on

studying primary vortex separation under steady and swept conditions for several angles of attack over a range of yaw angles from -20° to 25°. Comparison of flow visualization photographs at several angles of attack for yawed and zero sideslip cases provided the means to determine the effect of yaw on the flow field.

Flow visualization was used to study the effect of yaw on the flow field induced by a pitching cone-cylinder. Pictures for both the steady and the pitching cone-cylinder were taken at several angles of attack for positive and negative yaw angles. These angles of attack included angles resulting in symmetric vortex separation and angles resulting in asymmetric vortex separation. Smoke wire visualization in both the plane of and perpendicular to the pitching cylinder was effective in investigating the yaw effect on the model.

For the case when the cone-cylinder model was placed at a fixed angle of attack and yaw angle, the results suggest that the effective roll angle is the key parameter affecting vortex separation. When the cylinder was brought from $\alpha = 0^o$ to $\alpha = 56^o$ (asymmetric regime), the primary vortex was observed to separate outside of the yaw cone for all yaw angles investigated ($-20^o \setminus \beta \setminus 20^o$). However, when the cylinder was brought from $\alpha = 90^o$ to $\alpha = 56^o$, the primary vortex was observed to separate most of (but not all of) the time on the inside of the yaw cone. This result suggests a dependence on initial conditions. That is, for yaw angles of $|\beta| > 0^o$, the effective roll angle ϑ decreases in magnitude starting from $|\vartheta| = 90^o$ at $\alpha = 0^o$ for the case when the model is pitched from $\alpha = 0^o$ to $\alpha = 56^o$. However, when the cylinder is pitched from $\alpha = 90^o$ to $\alpha = 56^o$ for $|\beta| > 0^o$, the effective roll angle increases in magnitude starting at $\vartheta = \beta$ for $\alpha = 90^o$.

Another interesting result is that the flowfield about the model at a fixed angle of attack, was observed to be bistable at $\alpha=56^o$ for large yaw angles. The steady primary vortex could be made to separate on either side of the model. This was achieved by placing an obstruction upstream of the model causing the primary vortex to separate on a desired side of the model. Upon removal of this obstruction, the primary vortex was observed to continue to separate on the desired side. For a good discussion on this character of the flow field see Williams and Bernhardt (1990).

The present results also depict an effect of sweep rate on primary vortex separation. As the cylinder was swept from $\alpha = 0^o$ to 90^o for low sweep rates (positive sweep rate), the primary vortex was observed to separate on the outside of the yaw cone when the cylinder was passing through $\alpha = 56^o$. Note, this is the same result for the steady case when the cylinder was brought from $\alpha = 0^o$ to 56^o. As positive sweep rate was increased, primary vortex separation progressed from separation on the outside of the yaw cone ($\omega' = 0.056$) to symmetric shedding ($\omega' = 0.105$ and 0.140) and then to primary vortex shedding on the inside of the yaw cone for the higher sweep rate investigated ($\omega' = 0.175$).

Control of Asymmetric Vortices. Although many different methods of control have been demonstrated, our understanding of the details of the interaction between the control actuator and the flow is very limited. It is well known that the closer to the tip the actuator is located, the larger the control effect, but the scaling of the actuator size and forcing levels with various flight and vehicle parameters are not known. In this project the effects of Reynolds number on a suction and bleed control system have been studied. The level of suction required to control the flow is quantified, and a simple physical argument is proposed to explain the observed behavior. Such information is crucial to determining the forcing levels required to control the flow about full-scale aircraft.

At Reynolds number below 10,000 and for angles of attack greater than 50°, the side force exhibits a hysteresis loop in response to the control at the tip. The direction around the hysteresis

loop depends on the type of forcing, because the blowing and suction have opposite effects on the flow symmetry. When the vortex asymmetry is such that Cy<0, then the vortices can be switched by applying suction through the +135° side control holes or by applying blowing on the opposite side through the -135° side holes. This suggests that the flow (boundary layer) is thickened by the blowing and thinned by suction.

As the Reynolds number is increased, the hysteresis in the Cy vs Cb plot shrinks as described by Bernhardt and Williams (1993a). The response of the vortices changes from bi-stable behavior, to two-state to a continuous variation in Cy. The significance of these changes can be attributed to a change in the type of spatial instability governing the flow. One explanation for the hysteresis is pressure feedback from the wake to the tip of the model, which dominates the flow at low Reynolds number. The flow behaves like a global instability. Then the hysteresis disappears as the feedback decreases with increasing Reynolds number. Two stable states are found without a symmetric state. Further increases in Reynolds number lead to a continuous variation in Reynolds number. The flow behaves like a convective instability in response to forcing at the tip.

The control at the tip occurs through the changes in flow symmetry. Therefore, an important quantity is the level of forcing required to cause a jump from one stable state to another or to achieve the symmetric state, Cy=0. This is referred to as the critical bleed coefficient, Cb*. Regression analysis shows that Cb* is proportional to $Re^{3.9}$ (see Bernhardt and Williams 1993b). Then in terms of suction velocity, the critical suction speed u* is approximately proportional to U_o^3. It is not surprising that the level of forcing must increase as the flow speed increases.

The results give insight into the way in which blowing and suction change the flow symmetry. At some height y* in the undisturbed approaching boundary layer there will be a dividing streamline that separates the flow entering the slot from flow that passes over the top and continues on downstream. The height of the dividing streamline (or the distance to the stagnation point) can be used as a measure of the level of distortion created by the suction. Of course this is over-simplified for the three-dimensional flow about a small hole on a conical surface, but the basic concept is believed to be correct.

It has been shown that both suction and blowing are capable of controlling the asymmetric flow about the forebodies of aircraft and missiles, but the effects on flow asymmetry are opposite to each other. Experiments indicate that the suction bleed coefficient must increase like $U_o^{3.9}$ to balance the effect of the geometric instability at the tip.

E. Flow Control About Pitching Airfoils at High Angles of Attack

Within the past decade, there has been an impetus to develop flow-control systems to manage the unsteady separation over rapidly-pitching airfoils, thereby altering their aerodynamic behavior to increase aircraft maneuverability. Since the dynamic-stall vortex is one feature in this type of flow, the basis for any control strategy must rest on an understanding of the basic mechanisms that lead to its formation. The key to controlling the DSV lies in the ability to modify or suppress these mechanisms. By the time the stall vortex appears over the suction surface of the airfoil, it is too late to initiate any effective action to alter the flow. Any such action must be taken before this stage, during the nascent period of development of the DSV. It is thus necessary to understand the flow development in the *initial* stages of formation of the dynamic-stall vortex and identify the important mechanisms in this process. This essential step must be taken before it will be possible to develop techniques to identify the state of the flow, and to develop flow-control techniques that can be used to alter the flow state.

New experimental results, combined with recent theoretical advances in the understanding of unsteady, viscous flows have helped to develop a clearer picture of the phenomenon. The results summarized in this report are the outgrowth of an ongoing program at IIT to develop techniques for the real-time, reactive control of the dynamic-stall vortex over pitching airfoils. Since large-scale vortical structures dominate this flow, the evolution of the vorticity field must be examined carefully. The approach adopted has been to combine flow-visualization with quantitative measurements of the instantaneous surface pressure and vorticity flux to develop an understanding of this extremely complex flow field.

Acharya & Metwally (1992) describe experiments that provide important information about the evolution of unsteady pressure field and vorticity production over the airfoil surface. Acharya, Karim and Metwally (1993) describe the principal mechanisms in the initial stages of development of the dynamic-stall vortex and its subsequent evolution. A constant-velocity, large-amplitude pitch up of the airfoil in a steady oncoming stream is examined, since this is an appropriate airfoil motion for applications aimed at increasing aircraft maneuverability. Karim & Acharya (1993) report on one possible strategy for flow control using leading-edge suction. They examine the effectiveness of this approach to suppress, alter, delay, or otherwise control the formation of the DSV, and describe the influence of different parameters such as pitch rate, Reynolds number, suction timing, suction-slot size and slot location on the control of the DSV.

In the course of these investigations, the principal mechanisms contributing to the formation of the dynamic-stall vortex over a pitching airfoil, and the evolution of the vortex after it is formed, have been identified. The vorticity present in the dynamic-stall vortex originates from a concentrated source located on the pressure surface of the airfoil during most of the pitch up, and is transported over to the suction surface in a very thin shear layer. A thin region of near-wall, unsteady flow reversal in the forward portion of the airfoil results in the accumulation of fluid in the leading-edge region. The growth of this zone of accumulation of reverse-flow fluid causes the shear layer to be lifted up away from the airfoil surface. Accumulation of vorticity downchord of the zone of accumulation of reverse-flow fluid, coupled with a roll up of the shear layer leads to the formation of the dynamic-stall vortex. A simple model for the accumulation of reverse-flowing fluid is found to be valid at high pitch rates. The dynamic-stall vortex remains bound to the airfoil surface until a secondary flow eruption abruptly separates it from the shear layer, whereupon the vortex grows rapidly in size and convects downstream. The dynamic-stall vortex exhibits two distinct propagation velocities; one prior to, and one after detachment from the airfoil, and its movement over the airfoil is found to scale with the pitch rate. Trailing-edge flow reversal propagating upchord does not influence the formation or detachment of the dynamic-stall vortex,

but results in the formation of other vortical structures over the rearward part of the suction surface.

Experiments to control the dynamic-stall vortex (DSV) over the suction surface of a two-dimensional NACA 0012 airfoil, undergoing a 'hold-pitch-hold' motion, have been carried out. Measurements were performed over a range of Reynolds number ($3.0\times10^4 \leq Re_c \leq 11.8\times10^4$) and pitch rate ($0.072 \leq \alpha^+ \leq 0.31$), using leading-edge suction during a prescribed period of the airfoil motion. This strategy to manage the DSV, using controlled leading-edge suction, was developed from a study of the mechanisms responsible for the evolution of the vortex. The results indicate that formation of the DSV can be suppressed by removing an appropriate amount of the reverse-flowing fluid to prevent its accumulation in the near-leading edge region, thereby preventing lift up of the shear layer. The influence of different parameters such as pitch rate, Reynolds number, suction timing, and suction-slot size and location on the control of the DSV has been investigated. A scaling is developed for the suction flow rate which provides valuable information about the growth of the reverse-flow region and its dependency on different parameters. Parameter ranges are identified for which complete or partial suppression of the DSV can be achieved. Figure 12 shows the variation of required suction flow rate for complete suppression of the dynamic-stall vortex during a pitch-up motion, for different angles of attack and different pitch rates.

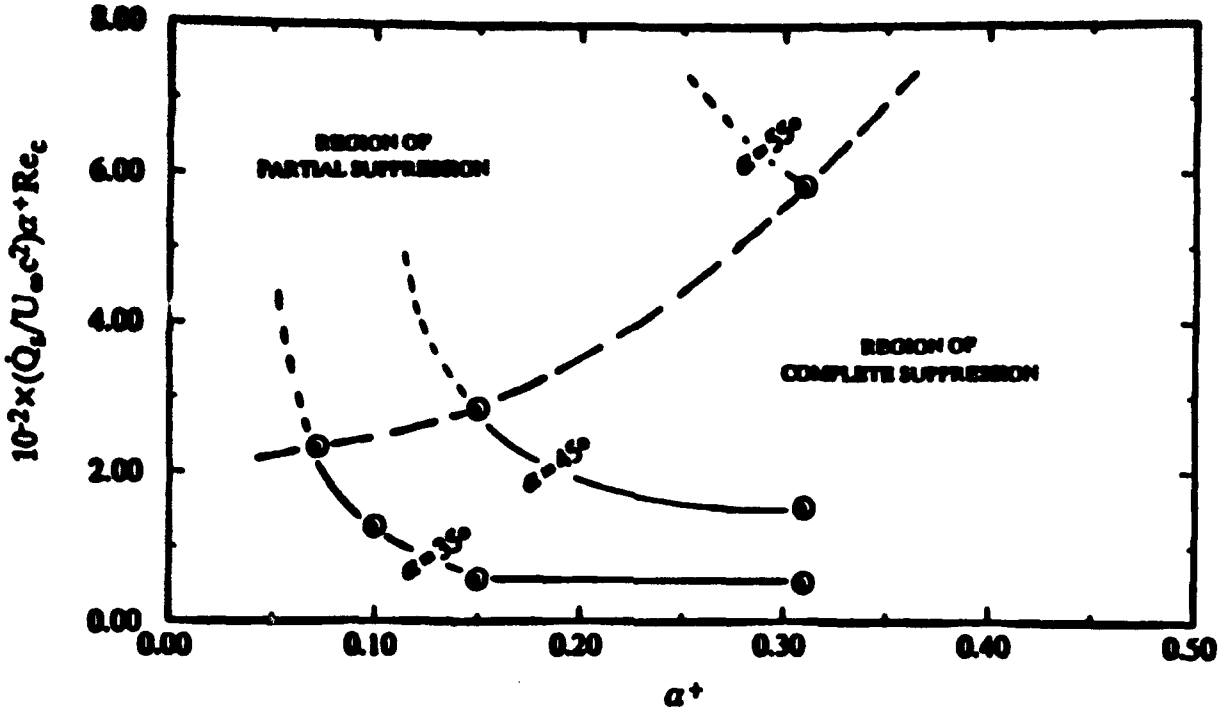

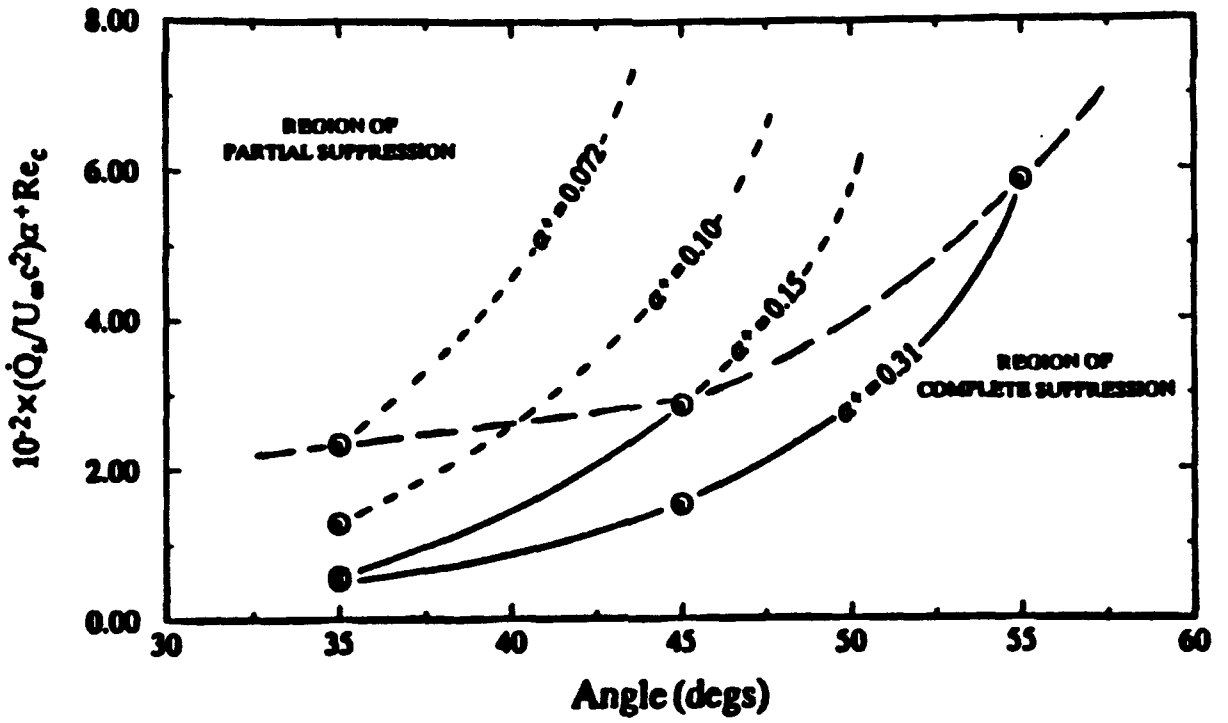

Figure 12 Variation of Suction Flow Rate for Complete Suppression of the DSV

F. The National Diagnostic Facility

During the three years of the Grant, this multi-year design and construction project was completed and initial documentation of the wind-tunnel flow quality was reported by Hites and Nagib (1993), and Nagib, Hites and Gravante (1993). The design of the facility began in the mid 1980s under AFOSR/URIP funding and construction started during the late 1980s under AFOSR/URI support. Tests in the facility are scheduled during 1994 for several AFOSR, ONR and ARO supported experiments in collaboration with several investigators from other laboratories including, University of Illinois at Urbana, University of Arizona, SUNY at Buffalo and Yale University.

The NDF has several features which make it particularly suitable for high Re fundamental research. The most substantial of which is the large, low-disturbance test section. The design of the facility includes a 4' x 5' x 35' (1.22 m x 1.52 m x 10.7 m) long test section with a maximum freestream velocity of 500 f/s (150 m/s). Other aspects of the test section include: clear glass doors over the full length, modular test section construction including a removable 9' (2.74 m) segment, motorized adjustable ceiling, a wide range of operating velocities, and steady-state temperature control at all freestream velocities.

This facility has been designed to insure quiet, low-disturbance, steady operation of the freestream. Flow is accelerated by a low RPM vane-axial fan which contributes a minimal amount of acoustic noise to the flow. Nevertheless, sound absorption is integrated into the turning vanes in turn two to further reduce acoustic disturbances. Large-scale turbulence downstream of turn two is manipulated by a single honeycomb section followed by a series of six fine-mesh screens. The contraction shape is given by a fifth order polynomial, and the temperature of the flow is maintained by a chilled water system which provides cooling through heat exchangers located in the turning vanes in turns one and three.

Preliminary turbulence measurements have been performed to evaluate the flow quality in the National Diagnostic Facility (NDF). Velocity and temperature were measured at different locations between the fan and test section of the NDF in order to quantify local turbulence levels. The temperature and velocity uniformity just upstream of the turbulence manipulators was found to be within 4% of freestream values. Analysis of hot-wire velocity timeseries showed that turbulence intensity was less than 1.5% far downstream of the honeycomb and less than 0.3% far downstream of the six screens. Calculation of power spectra demonstrated a smooth broadening of turbulence spectra with mean freestream velocity and a shear layer instability characteristic frequency of about 2300 Hz for the screens. The combination of these results have verified the effectiveness of the turbulence manipulators in the NDF. Moreover, with the further reductions in disturbance level anticipated with the addition of the contraction, it is expected that the test section freestream turbulence intensity should be in the range $0.03\% < u'/U < 0.05\%$.

National Diagnostic Facility

Illinois Institute of Technology

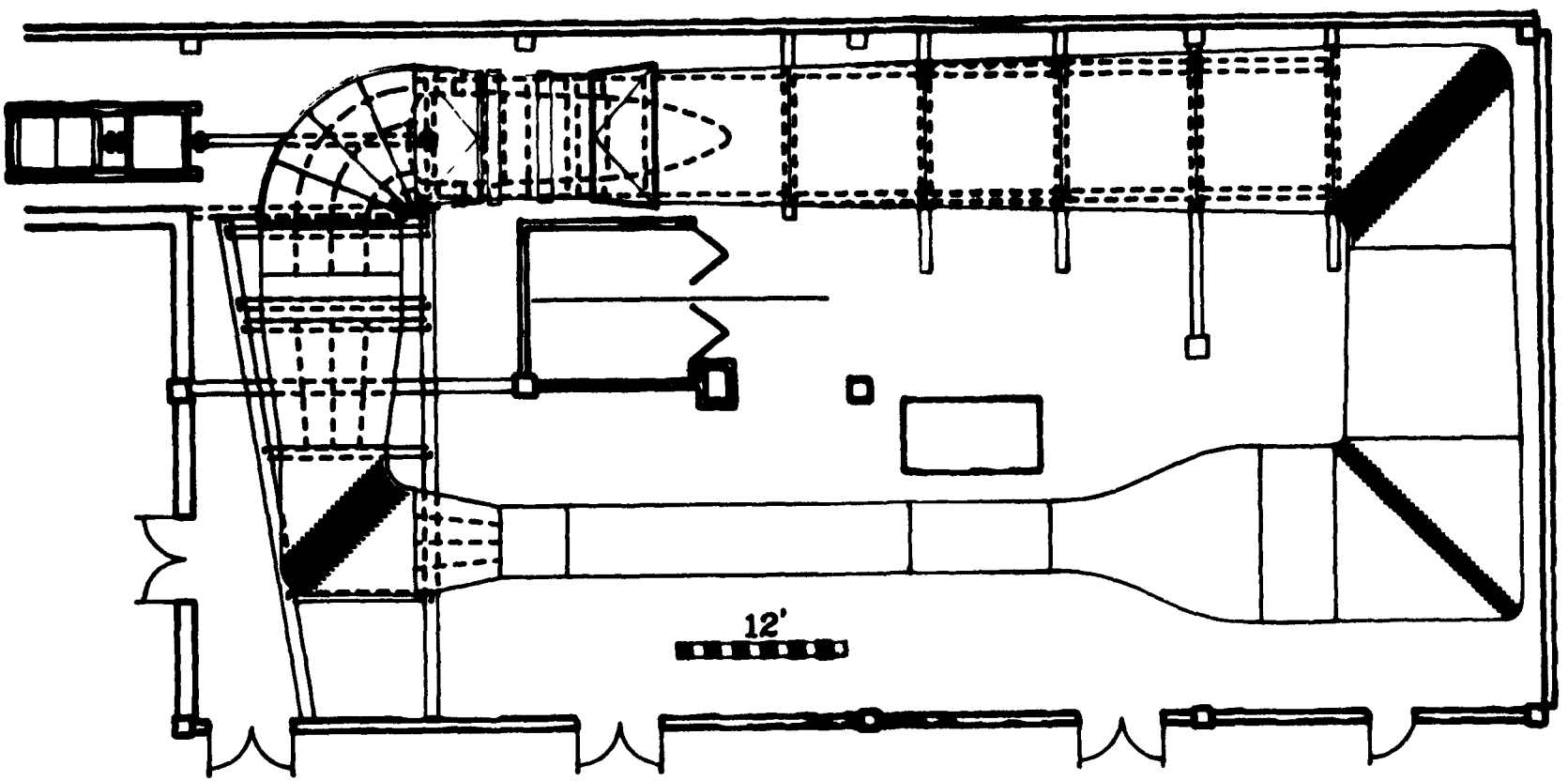

Figure 13 Plan view schematic of National Diagnostic Wind Tunnel.

References

Acharya M. & Metwally, M. H. 1992 "Unsteady pressure field and vorticity production over a pitching airfoil." AIAA Journal 30, no. 2, 403-411.

Acharya, M., Karim M. A. & Metwally M. H., 1993 "Development of the dynamic-stall vortex over a pitching airfoil." Submitted for publication.

Bernhardt, J.E. & Williams, D. R. 1993a "The effect of Reynolds number on vortex asymmetry about slender bodies." Phys. Fluids A 5, no. 2, 291-293.

Bernhardt, J.E. & Williams, D. R. 1993b "The effect of Reynolds number on Control of Forebody Asymmetry by Suction and Bleed." AIAA Shear Flow Conference. AIAA 93-3265.

Corke, T. C., and Mangano, R.A., 1989. "Resonant growth of three-dimensional modes in transitioning Blasius boundary layers." J. Fluid Mech., 50, p. 93.

Corke, T. C., 1989. "Resonant three-dimensional boundary layers structure and control." AIAA Shear Flow Control Conference. AIAA-89-1001.

Corke, T. C., 1990. "Effect of controlled resonant interactions and mode detuning on turbulent transition in boundary layers." IUTAM Symposium on Laminar-Turbulent Transition, Springer-Verlag, p 151.

Corke, T. C., Shakib, F. and Nagib, H. 1991. "Mode selection and resonant phase locking in unstable axisymmetric jets." J. Fluid Mech., 223, 253-311.

Corke, T. C. and Kusek, S. M. 1992. "Resonance in axisymmetric jets with controlled helical mode input." J. Fluid Mech, 249, 307-336.

Choudhari, M., "Distributed Acoustic Receptivity in Laminar Flow control Configurations," Contract Report NASA-CR 4438, 1992.

Craik, A. D. D., 1971. "Nonlinear resonant instability in boundary layers." J. Fluid Mech., 50, p. 393.

Crouch, J. D., "Nonlocalized Receptivity of Boundary Layers," Submitted to J. Fluid Mech., 1990.

Crouch, J. D. and Bertolotti, F. P., "Nonlocalized Receptivity of Boundary Layers to Three-Dimensional Disturbances," AIAA 92-0740, 1992.

Choudhari, M., "Boundary-Layer Receptivity due to Distributed Surface Imperfections of a Deterministic or Random Nature," Theoret. Comput. Fluid Dynamics, 4, 101-118, 1993.

Herbert, Th. 1983. (a) Secondary Instability of plane channel flow. Phys. Fluids, 26, p. 871.

Hites, M. and Nagib, H., "Measurement of Disturbance Levels in the National Diagnostic Facility," AIAA 94-0770, AIAA Aerospace Science Meeting, Reno, NV, 1994.

Kachanov, Yu. S. and Levchenko, V. Ya., 1984. "The resonant interaction of disturbances at laminar- turbulent transition in a boundary layer." J. Fluid Mech., 138, p. 209.

Karim, M. A. & Acharya, M. 1993 "Control of the dynamic-stall vortex over a pitching airfoil by leading-edge suction." AIAA Paper 93-3267.

Keener, E. R. and Chapman, G. T. 1974. "Onset of aerodynamic side forces at zero sideslip on symmetric forebodies at high angles of attack." AIAA Paper No. 74-770. Proceedings of the AIAA Mechanics and Control of Flight Conference, Anaheim, California, August 5-9.

Keener, E. R., Chapman, G. T. and Kruse, R. L. 1976. "Effects of Mach number and afterbody length on onset of asymmetric forces on bodies at zero sideslip and high angles of attack." AIAA Paper No. 76-66. Proceedings of the AIAA 14th Aerospace Sciences Meeting, Washington, D. C., January 26-28.

Klebanoff, P. S., Tidstrom, K. D. and Sargent, L. M. 1962. "The three-dimensional nature of boundary layer instability". J. Fluid Mech., 12, p. 112.

Koratagere, S. 1990. "Broad-band 3-D mode development in a Blasius boundary layer by resonant mode detuning." M.S. Thesis, Illinois Institute of Technology.

Mankbadi, R. and Liu, J. 1981. "A study of the interactions between large large-scale coherent structures and fine-grained turbulence in a round jet." Philos. Trans. R. Soc. London Ser. A, 298, 541-602.

Montividas, R. E. 1988. The Scaling and Control of Vortex Geometry behind Pitching Bodies of Revolution. M.S. Thesis, Illinois Institute of Technology, Chicago, Illinois.

Nagib, H., Hites, M., and Gravante, S., "Flow Quality Documentation of the National Diagnostic Facility," to be presented at the 18th AIAA Aerospace Ground Testing Conference, Colorado Springs, CO, 1994.

Santos, G.R. 1987. Studies on Secondary Instabilities. Ph.D thesis, Virginia Polytechnic and State University.

Santos, G.R. and Herbert, Th. 1986 "Combination resonance in boundary layers." Bull. Am. Phys. Soc. 31:1718.

Williams, D. R. and Bernhardt J. 1990. "Proportional control of asymmetric forebody vortices with the unsteady bleed technique." AIAA Paper No. 90-1629, Proceedings of the AIAA 21st Fluids Dynamics, Plasma Dynamics and Lasers Conference, Seattle, Washington, June 18-20.

Vial, S.Y.R. 1990. Effect of Yaw on a Pitching Cone-Cylinder. M.S. Thesis, Illinois Institute of Technology, Chicago, Illinois.

Zavol'skii, N.A., Reutov, V.P., and Ryboushkina, G.V., "Generation of Tollmien-Schlichting Waves via Scattering of Acoustic and Vortex Perturbations in Boundary Layer on Wavy Surface," J. Appl. Mech. Tech. Phys., pp. 79-86, 1983.

List of Publications

Acharya M. & Metwally, M. H. 1992 Unsteady pressure field and vorticity production over a pitching airfoil. AIAA Journal, 30, no. 2, 403-411.

Acharya, M., Karim M. A. & Metwally M. H., 1993 Development of the dynamic-stall vortex over a pitching airfoil. Submitted for publication.

Bernhardt, J.E. & Williams, D. R. 1993a "The effect of Reynolds number on vortex asymmetry about slender bodies." Phys. Fluids A 5, no. 2, 291-293.

Bernhardt, J.E. & Williams, D. R. 1993b "The effect of Reynolds number on Control of Forebody Asymmetry by Suction and Bleed." AIAA Shear Flow Conference. AIAA 93-3265.

Corke, T. C., Shakib, F. & Nagib, H. 1991. Mode selection and resonant phase locking in unstable axisymmetric jets. J. Fluid Mech., 223, 253-311.

Corke, T. C. & Kusek, S. M. 1992. Resonance in axisymmetric jets with controlled helical mode input. J. Fluid Mech., 249, 307-336.

Corke, T.C., 1990. Effect of controlled resonant interactions and mode detuning on turbulent transition in boundary layers. IUTAM Symposium on Laminar-Turbulent Transition, Springer-Verlag, p 151.

Corke, T.C. 1993. Three-dimensional mode growth in boundary layers with tuned and detuned subharmonic resonance. To appear Royal Soc. Trans. A.

Hites, M. and Nagib, H., "Measurement of Disturbance Levels in the National Diagnostic Facility," AIAA 94-0770, AIAA Aerospace Science Meeting, Reno, NV, 1994.

Nagib, H., Hites, M., and Gravante, S., "Flow Quality Documentation of the National Diagnostic Facility," to be presented at the 18th AIAA Aerospace Ground Testing Conference, Colorado Springs, CO, 1994.

Nagib, H. "A National Low Disturbance Subsonic Tunnel," AIAA 92-3911, 17th AIAA Aerospace Ground Testing Conferenc, Nashville, TN, 1992.

Reisenthel, P., Nagib, H. & Nivelet, N. 1993. Closed-Loop Excitation of an Axisymmetric Free Jet., submitted to Phys. Fluids A., after presentation at Special Conference in Honor of Professor W. C. Reynolds, March, 1993.

Wiegel, M. and Wlezien, R. W., "Acoustic Receptivity of Laminar Boundary Layers over Wavy Walls", AIAA Paper No. 93-3280, AIAA Shear Flow Conference July 6-9, 1993, Orlando, FL.

Williams, D. R. and Bernhardt J. 1990. "Proportional control of asymmetric forebody vortices with the unsteady bleed technique". AIAA Paper No. 90-1629, Proceedings of the AIAA 21st Fluids Dynamics, Plasma Dynamics and Lasers Conference, Seattle, Washington, June 18-20.

Students, Post Docs and Other Investigators Supported

Students Supported, Graduation Year:

M.S. Students:

Md. Ahsan Karim, 1992.
S. Korategere, 1990.
Steve Kusek, 1990.
Sophie Vial, 1990.
Markus Wiegel, 1993.

Ph.D. Students:

Sang Ahn, 1994.
John Bernhardt, 1994.
Metwally H. Metwally, 1991

Post-Docs and Other Investigators Supported:

Patrick H. Reisenthel
Richard W. Wlezien